HHS Public Access

Author manuscript

Biomaterials. Author manuscript; available in PMC 2019 April 01.

Published in final edited form as:

Biomaterials. 2018 April ; 160: 24–36. doi:10.1016/j.biomaterials.2018.01.012.

Biomimetic and enzyme-responsive dynamic hydrogels for studying cell-matrix interactions in pancreatic ductal adenocarcinoma

Hung-Yi Liu[1], **Murray Korc**[2,3], and **Chien-Chi Lin**[1,3,4,*]

[1]Weldon School of Biomedical Engineering, Purdue University, West Lafayette, IN 47907, USA

[2]Department of Medicine and Biochemistry & Molecular Biology, Indiana University School of Medicine, Indianapolis, IN 46202, USA

[3]Indiana University Melvin and Bren Simon Cancer Center and The Pancreatic Cancer Signature Center, Indianapolis, IN 46202, USA

[4]Department of Biomedical Engineering, Purdue School of Engineering & Technology, Indiana University-Purdue University Indianapolis, Indianapolis, IN 46202, USA

Abstract

The tumor microenvironment (TME) governs all aspects of cancer progression and *in vitro* 3D cell culture platforms are increasingly developed to emulate the interactions between components of the stromal tissues and cancer cells. However, conventional cell culture platforms are inadequate in recapitulating the TME, which has complex compositions and dynamically changing matrix mechanics. In this study, we developed a dynamic gelatin-hyaluronic acid hybrid hydrogel system through integrating modular thiol-norbornene photopolymerization and enzyme-triggered on-demand matrix stiffening. In particular, gelatin was dually modified with norbornene and 4-hydroxyphenylacetic acid to render this bioactive protein photo-crosslinkable (through thiol-norbornene gelation) and responsive to tyrosinase-triggered on-demand stiffening (through HPA dimerization). In addition to the modified gelatin that provides basic cell adhesive motifs and protease cleavable sequences, hyaluronic acid (HA), an essential tumor matrix, was modularly and covalently incorporated into the cell-laden gel network. We systematically characterized macromer modification, gel crosslinking, as well as enzyme-triggered stiffening and degradation. We also evaluated the influence of matrix composition and dynamic stiffening on pancreatic ductal adenocarcinoma (PDAC) cell fate in 3D. We found that either HA-containing matrix or a dynamically stiffened microenvironment inhibited PDAC cell growth. Interestingly, these two factors synergistically induced cell phenotypic changes that resembled cell migration and/or invasion in 3D. Additional mRNA expression array analyses revealed changes unique to the presence of HA, to a stiffened microenvironment, or to the combination of both. Finally, we

*To whom correspondence should be sent: Chien-Chi Lin, PhD., Associate Professor Department of Biomedical Engineering Purdue School of Engineering & Technology Indiana University-Purdue University Indianapolis Indianapolis, IN 46202 Phone: (317) 274-0760, lincc@iupui.edu.

presented immunostaining and mRNA expression data to demonstrate that these irregular PDAC cell phenotypes were a result of matrix-induced epithelial-mesenchymal transition (EMT).

Keywords

Pancreatic ductal adenocarcinoma; dynamic hydrogel; matrix stiffness; hyaluronic acid; epithelial-mesenchymal transition

Introduction

Pancreatic cancer is currently the third leading cause of all cancer-related deaths. More than 53,000 new pancreatic cancer cases and 43,000 deaths are projected in 2017 [1]. The exceptionally dense stromal tissue (i.e., desmoplasia) in pancreatic ductal adenocarcinoma (PDAC), the most common form of pancreatic cancer, is considered the major hurdle to effective treatments [2]. Pancreatic desmoplasia is rich in extracellular matrix (ECM) proteins (e.g., collagen, fibronectin), glycosaminoglycans (GAGs, e.g., hyaluronic acid (HA)), cytokines (e.g., epidermal growth factor (EGF), transforming growth factor-β (TGF-β)), as well as immune and stromal cells [3-6]. The compositions in the stroma tissue act collectively to induce epithelial-mesenchymal transition (EMT) in cancer cells [7]. EMT is a complex process regulated by interactions of cancer-stromal cell, as well as bi-directional signaling between cancer cells and the surrounding tumor matrix [8, 9]. For example, inflammatory cytokines and growth factors, including TGF-β and EGF, are known to promote EMT in PDAC cells [9-12]. These cytokines are abnormally expressed during tumor progression, leading to downregulation of epithelial markers (e.g., E-Cadherin) and upregulation of mesenchymal markers (e.g., N-Cadherin, SNAIL, TWIST, SLUG, ZEB1, etc.) [13, 14]. Under the stimulation of abnormally expressed cytokines, PDAC cells lose cell-cell junctions and transform into cells with a migratory and invasive phenotype. Moreover, these cellular changes render cancer cells chemo-resistant [7, 13, 15, 16].

In addition to soluble cytokines, many ECM components are overexpressed by stromal and cancer cells during tumor progression. The accumulation of ECM proteins and GAGs around cancer cells builds up a dense desmoplasia that not only physically restricts penetration of chemotherapeutics but also causes abnormal mechanotransduction in cancer cells [17, 18]. For example, excessive accumulation of HA was detected in cell culture and in mature PDAC stroma [19]. HA binds to cell surface receptors, including CD44, layilin, and receptor for hyaluronan-mediated motility (RHAMM) [19-21]. The activation of these receptors has been positively correlated with enhanced cancer cell proliferation, invasion, and drug resistance [22]. In addition, HA accumulation also leads to elevated fluid stress that could induce abnormal mechanosensing in the cancer cells and limit the transport of anti-cancer drugs [23, 24]. Nonetheless, the roles of HA in a stiffening microenvironment on PDAC cell EMT have not been extensively studied owing to the lack of an appropriate three-dimensional (3D) culture system capable of mimicking the dynamic stroma stiffening process.

To investigate cancer cell responses induced by ECM, most studies utilized two-dimensional (2D) tissue culture plate coated with matrix proteins or 3D hydrogels with static or

degrading mechanical property [25]. Unfortunately, these convenient culture platforms do not capture the dynamic landscape of a stiffening tumor microenvironment (TME). Some dynamic hydrogels have been developed to mimic the temporal mechanical changes of tumor matrix. For example, Suggs and colleagues developed an alginate-based hydrogel that could be dynamically stiffened by temperature-induced calcium release [26]. MCF10A mammary epithelial cells, which are non-tumorigenic, were nonetheless found to exhibit an invasive phenotype when cultured in a stiffened matrix, a result consistent with earlier work [27, 28]. In another example, Xu *et al.* developed a double-network dynamic hydrogel via a two-step light-mediated polymerization process [29]. Methacrylate and cysteine dually functionalized HA was crosslinked into hydrogels through ultraviolet (UV) light polymerization, followed by infiltrating the hydrogel with additional macromers, photoinitiators, and secondary UV light-mediated polymerization. The authors concluded that encapsulated cancer cells became invasive in the stiffened gel. Although these strategies presented dynamic matrix stiffening, the components and approaches were either not biologically relevant to the TME due to the inclusion of alginate, or exposed cells to UV light excessively.

Our group has reported several semi-synthetic poly(ethylene glycol) (PEG)-peptide hydrogels for *in vitro* culture of pancreatic cancer cells [10, 30-32]. For example, we have evaluated PDAC cell EMT in hydrogels immobilized with fibronectin or laminin-derived peptides [31]. We have also studied the influence of matrix-entrapped collagen-1 and soluble cytokines (e.g., TGF-β1 and EGF) on PDAC cell fate, including proliferation, chemo-resistance, and EMT in 3D [30]. In order to mimic the dynamic tumor stromal tissue, we have recently developed a tyrosinase-triggered post-gelation crosslinking platform for on-demand stiffening of cell-laden hydrogels [33]. These hydrogels were prepared by thiol-norbornene photopolymerization using 8-arm PEG-norbornene (PEG8NB) and a simple peptide linker (i.e., KCYGPQGIWGQYCK) sensitive to both matrix metalloproteinase (MMP) induced cleavage and tyrosinase-triggered di-tyrosine crosslinking. Following thiol-norbornene gelation, the tyrosine residues in the primary network served as substrates for exogenously added tyrosinase, which catalyzes di-tyrosine crosslinking and increases hydrogel crosslinking density and stiffness. Furthermore, enzyme-triggered on-demand stiffened hydrogels altered morphology of pancreatic stellate cells (PSCs) cultured in 3D and resulted in upregulation of α-smooth muscle actin (αSMA), a signature marker of myofibroblastic activation.

Although the tyrosinase-stiffened PEG-peptide hydrogels have been useful in studying the effect of dynamic matrix stiffening on cancer stromal cell fate, these gels represented minimal tumor-related matrix components. In a separate study, our group designed biomimetic hydrogels formed by visible light initiated crosslinking of gelatin-norbornene (GelNB) and thiolated HA (THA) [32]. These gels were established to understand the effect of individual matrix component and static gel stiffness on PDAC cells grown in 3D but did not encompass dynamic stiffening feature. Here, we present a pathophysiologically relevant dynamic biomimetic hydrogel system where the gel network was formed by THA and dually-functionalized gelatin. The later was chemically modified with norbornene (NB) and hydroxyphenylacetic acid (HPA), yielding a multifunctional and cell responsive macromer (i.e., GelNB-HPA). Through orthogonal thiol-norbornene photopolymerization, GelNB-HPA

were modularly crosslinked by THA or by inert macromer PEG-tetra-thiol (PEG4SH). The bioactive peptide sequences on gelatin permitted cell adhesion and MMP-mediated local matrix cleavage. The conjugated HPA moieties rendered the cell-laden hydrogels sensitivity to tyrosinase-triggered di-HPA crosslinking, which led to physiologically relevant degree of on-demand stiffening in the presence of PDAC cells. With this new hybrid biomimetic hydrogel system, the effects of matrix biochemical and biophysical cues could be easily decoupled for gaining new insights into the effects of matrix compositions on PDAC cell behavior. We systematically characterized gel crosslinking and enzyme-triggered stiffening and degradation. We also studied the independent and synergistic effects of matrix compositions and dynamic stiffening on PDAC cell fate in 3D by analyzing cell morphological changes, immunostaining, and expression of PDAC-related genes at the mRNA level. Through modularly crosslinking and dynamically stiffening of tumor-mimetic matrices, we discovered the unique role of HA on PDAC cell fate processes and modulation of gene expression.

Materials & Methods

Materials

Gelatin type B, THA (MW: ~300 kDa), and PEG4SH (MW: 10 kDa) were obtained from Electron Microscopy Sciences, ESI Bio, and JenKem Technology USA, respectively. Collagenase-1 (300 U/mg) and hyaluronidase (770 U/mg) were purchased from Worthington Biochemical. All the other chemicals were obtained from Thermo Fisher unless noted otherwise.

Synthesis of functionalized gelatin macromers

The synthesis of GelNB-HPA was achieved in two steps. First, gelatin-norbornene (GelNB) was synthesized by reacting gelatin with carbic anhydride as described previously [34]. The second functional group, HPA, was conjugated on the remaining amine groups on GelNB through standard carbodiimide chemistry with 1-ethyl-3-(3-dimethylaminopropyl)-carbodiimide (EDC) and N-hydroxysuccinimide (NHS) as the coupling reagents [35]. The reaction was carried out for 24 hours and the degree of substitution was determined using fluoraldehyde assay with unmodified gelatin as the standards. The functionalization was also characterized by UV/Vis spectrophotometry (Synergy HT microplate reader, BioTek Instruments) and ^{1}H NMR (Avance III 500, Brüker).

Hydrogel fabrication and characterization

Hydrogels were prepared by reacting norbornene moieties of functionalized gelatin with thiol motifs on PEG4SH or THA via thiol-norbornene photopolymerization [36, 37]. Briefly, precursor solutions (45 μl/gel) composed of macromers and photoinitiator lithium acylphosphinate (LAP, 1 mM) were injected between two glass slides separated by 1-mm thick spacers. Gelation was achieved in 2 minutes under 365 nm light exposure (5 mW/cm^2). Hydrogels were swollen in DPBS at 37°C for 2 hours prior to characterization or stiffening experiments. Gelation kinetics and mechanical properties of hydrogels were characterized with a digital rheometer (Bohlin CVO100, Malvern Instruments). *In situ* gelation was performed in time-sweep mode using 10% strain, 1 Hz frequency, and a gap size of 90 μm.

Hydrogel bulk moduli were obtained from averaging the linear region of the modulus-strain curves in strain-sweep mode (8 mm parallel plate geometry with a gap size of 700 μm).

Tyrosinase-triggered on-demand gel stiffening

Tyrosinase-triggered hydrogel stiffening was performed by incubating the pre-formed hydrogels in tyrosinase solution as described previously [33]. Afterwards, gels were transferred to DPBS (for cell-free gels) or fresh media (for cell-laden gels) in order to remove the residual tyrosinase trapped in the hydrogels.

Enzymatic degradation of soft and stiffened hydrogels

Collagenase-1 and hyaluronidase were used to evaluate the susceptibility of the hydrogels to on-demand enzymatic degradation. Briefly, hydrogels were prepared with or without TYR-triggered stiffening as described in the section above. The gels were incubated in DPBS for one day prior to gravimetrically weighing to determine the initial gel mass (M_0). Next, gels were incubated in respective enzyme solution for predefined periods of time and weighed to obtain current mass (M_t) and to determine percentage of mass loss (i.e., $100\% \times (M_0 - M_t)/M_0$). The degradation process was continued until the gels were completely degraded or no substantial changes in mass loss were observed.

PDAC cell culture, encapsulation, and characterizations

COLO-357, a PDAC cell line with wild-type *KRAS*, was maintained in high glucose DMEM supplemented with 10% of fetal bovine serum (FBS, Gibco) and penicillin-streptomycin (Gibco, 50 U/mL for both antibiotics). Cells were maintained in a standard cell culture incubator (37°C, 5% CO_2). Prior to encapsulation, cells were trypsinized and suspended in precursor solutions (to 2×10^6 cells/mL) composed of photoinitiator LAP and required macromers (i.e., PEG4SH, THA, GelNB, or GelNB-HPA at desired concentrations as denoted in each Figure). Cell-precursor solution (25 μL) was loaded to a 1 mL disposable syringe with cut-open tip and exposed to 365 nm light (5 mW/cm^2) for 2 minutes. Cell-laden hydrogels were cultured in a 24-well plate. To evaluate cells viability, cell-laden gels were stained with live/dead staining kit (Life Technologies; Calcein-AM stained live cells green, Ethidium homodimer-1 stained dead cells red) and imaged via confocal microscopy (Olympus Fluoview FV100 laser scanning microscope). Z-stack images (100 μm thick, 10 μm per slice) were obtained from a minimum of three random areas within hydrogels. In addition, cells metabolic activity was obtained by using AlamarBlue assay (AbD Serotec; 10% in culture media, 2.5 hours of incubation time) and quantified via a microplate reader (Synergy HT, BioTek). Additional cell encapsulation studies were conducted using another human PDAC cell line, PANC-1, which harbors mutated *KRAS*.

RNA Isolation, reverse transcription PCR, and real-time PCR

Samples of cell-laden hydrogels were collected in DNase/RNase-free microtubes, flash-frozen in liquid nitrogen and stored in −80°C. Tota l RNA was isolated from the encapsulated cells with NucleoSpin RNA II kit (Clontech). The concentration and purity of RNA were obtained by NanoDrop 2000 Spectrophotometer (Thermo Scientific). Next, purified RNA samples were converted into complementary DNA (cDNA) with PrimeScript

RT Reagent Kit (Clontech, TaKaRa). For Taqman® array experiments, only samples with concentration greater than 100 ng/mL, 260/280 > 2.0, 260/230 > 1.8 were used. cDNA samples were diluted to 100 ng/mL and mixed with same volume of Taqman® fast universal master mix. For 96 well TaqMan® Array Gene Signature Sets, 10 μl mixture was deposited in each well and detected by Applied Biosystems 7500 Fast Real-Time PCR machine. Three biological replicas were used for each experimental condition. Additional qPCR on EMT-related genes was performed using cDNA and SYBR Premix Ex TaqII kit (Clontech) with appropriate primers as listed in Table S1. The relative gene expression levels were analyzed by the $2^{-\Delta\Delta CT}$ method with GAPDH as the internal control (i.e., housekeeping gene) and the expression level of respective gene in the control group (i.e., Gel/PEG gel with no HA and no stiffening) as the external control.

Immunofluorescence staining and imaging

F-actin staining was used to visualize cytoskeletal structure of cells encapsulated in 3D environment with different matrix properties. Briefly, encapsulated cells were fixed in 4% paraformaldehyde for an hour at room temperature on an orbital shaker. Following fixation, samples were rinsed with DPBS and permeabilized with 1 mg/mL saponin at room temperature for 45 min. The samples were then washed with DPBS and blocked with 1% BSA and 10% FBS overnight at 4°C with shaking. The gels were then i ncubated overnight at 4°C in phalloidin solution (100 nM) and then washed with DPBS. Cell nuclei were counter-stained with DAPI (1:1000) for an hour at room temperature and rinsed three times with DPBS. Z-stack images (15 μm thick, 1 μm per slice) were obtained with a confocal microscope. To examine potential EMT in the encapsulated cells, E-cadherin (E-cad) and N-cadherin (N-cad) were stained by immunofluorescence. In brief, cell-laden gels were fixed, permeabilized, and blocked as described previously [38], followed by incubation with Rabbit anti-E-cad (1:100) and Mouse anti-N-cad (1:100) at 4°C for two days. After washing with DPBS extensively, samples were incubated with goat anti-Rabbit IgG (H+L)-Texas red or Alexa Fluor® 488-labeled goat anti-mouse IgG $F(ab')^2$ for two days at 4°C with gently shaking. Following by rinsing with DPBS and counter-staining with DAPI (1:1000), the samples were imaged by z-stack images (25 μm thick, 1 μm per slice) confocal microscopy with appropriate filters.

Statistical Analysis

All experiments were conducted independently three times with a minimum of three samples per condition. Numerical data were analyzed with two-way ANOVA on GraphPad Prism 7 software and reported as mean ± SEM. Single, double, and triple asterisks represent $p < 0.05$, 0.001, and 0.0001, respectively. $p < 0.05$ was considered statistically significant. For analyzing of Taqman® mRNA expression array, pairs of groups were compared with one-way ANOVA using Gel/PEG gels as the control (IBM SPSS software), following by Bonferroni post-analysis (Table S2, S3).

Results

Principles of dynamic hydrogel design and macromer synthesis

In order to recapitulate the bioactive components and the stiffening tumor microenvironment in PDAC (Fig. 1A), we prepared gelatin-hyaluronic acid (Gel/HA) hydrogels capable of undergoing on-demand stiffening. We synthesized GelNB and GelNB-HPA (Fig. 1B), which could be modularly crosslinked with commercially available THA (Fig. 1C) through thiolnorbornene photopolymerization. GelNB-HPA was synthesized through sequentially reacting gelatin with carbic anhydride (yielding GelNB) and 4-HPA (yielding GelNB-HPA). The degrees of gelatin functionalization, as characterized by fluoraldehyde assay, was ~37% and ~41% respectively for NB and HPA modification (equivalent to 1.6 mM NB and 1.64 mM HPA per wt% gelatin, data not shown). The presence of NB group on gelation permitted rapid gelation with THA (within 2 minutes) through orthogonal thiol-norbornene photopolymerization (Fig. 1D). When GelNB-HPA was used, the gels could be dynamically stiffened due to tyrosinase-triggered HPA dimerization (Fig. 1E).

Successful conjugation of NB and HPA moieties was characterized by ^{1}HNMR (Fig. 2A). Chemical shifts between 6.1 – 6.3 ppm (blue region) indicated successful NB functionalization on the gelatin backbone (7.2 – 7.4 ppm, green region). After HPA conjugation, new chemical shifts emerged (6.9 – 7.2 ppm, red region) in GelNB-HPA, indicating the presence of aromatic HPA [39]. The modification of HPA on GelNB was further confirmed by UV/Vis absorbance spectrometry (Fig. 2B) through detecting increased absorbance at 280 nm [40]. UV/Vis spectrometry were also used to monitor tyrosinase-triggered HPA dimerization. Due to the limited amount of tyrosine residue in the unmodified gelatin sequence (<0.5%) [41], addition of tyrosinase (TYR, 1 kU/mL) did not change the absorbance signature of GelNB significantly (Fig. 2C). However, when GelNB-HPA was treated with TYR, new absorbance shoulder emerged at ~320 nm (Fig. 2D), suggesting that HPA motifs were dimerized by tyrosinase [42].

Gel crosslinking and tyrosinase-mediated dynamic stiffening

To evaluate if conjugation of HPA on GelNB altered the efficiency of light-mediated thiol-norbornene photopolymerization, we conducted *in situ* photorheometry using GelNB or GelNB-HPA (7 wt%) and with PEG4SH (1.4 wt%) as the thiol crosslinker. As shown in Fig. 3A and 3B, gel points (i.e., storage modulus G' surpassed loss modulus G'') were ~9 and ~18 seconds for gelation using GelNB and GelNB-HPA, respectively. However, G' reached plateau within 2 minutes for both gelatin macromers. Furthermore, gels prepared from GelNB-HPA had lower moduli (~1 kPa) compared with gels crosslinked by GelNB (~1.7 kPa). Hydrogels crosslinked by GelNB-HPA and PEG4SH were used to evaluate the efficiency of tyrosinase-triggered on-demand stiffening. As shown in Fig. 3C, gel moduli did not change overtime when the solution contained no TYR. Gel moduli only increased slightly when incubating with low TYR concentration (0.1 kU/mL) for 4 hours. When TYR concentration was increased to above 0.5 kU/mL, hydrogels were significantly stiffened after only two hours of incubation. The color of gels treated with higher TYR concentrations was darker (Fig. 3D), indicative of HPA dimer formation and higher degree of stiffening.

In addition to TYR concentration, HPA contents in the hydrogel could also be modularly adjusted to control the degree of stiffening. As shown in Fig. 4A, hydrogels formed with pure GelNB (i.e., 0% GelNB-HPA) were not susceptible to TYR-triggered stiffening. However, when the amount of GelNB-HPA was modularly increased to 50% (i.e., half GelNB, half GelNB-HPA) and 100% (i.e., pure GelNB-HPA), gel were stiffened from ~1 kPa to ~2.2 kPa and ~2.9 kPa, respectively. We further adjusted the weight percentages of GelNB-HPA (e.g., 3, 5, 7 wt%) and PEG4SH (e.g., 0.6, 1, 1.4 wt%) in the macromer precursor solution to obtain gels with varying HPA contents but similar initial shear moduli (~1 kPa. Fig. 4B). Following tyrosinase treatment, gels with higher HPA content (i.e., 11.2 mM in 7 wt% GelNB-HPA) were stiffened to a higher degree (~2.7 kPa, Fig. 4B). We also prepared gels with different thiol/norbornene stoichiometric ratio ($R_{thiol/ene}$) but with the same HPA contents (i.e., 7 wt% GelNB-HPA and PEG4SH at 0.8, 1.4, 2, or 2.8 wt%. Fig. 4C). There was a positive correlation between $R_{thiol/ene}$ and initial gel modulus and these gels could all be dynamically stiffened regardless of the initial moduli (Fig. 4C). Most importantly, once stiffened by TYR (1 kU/mL), all gels remained stiff for the next few days and the degree of stiffening (~1 kPa to ~8 kPa) was relevant to the stiffness change in a stiffening TME [43].

Enzyme-mediated degradation of soft and stiffened hydrogels

Owing to the use of naturally derived macromers (i.e., gelation and HA), this hydrogel system was susceptible to degradation by cell-secreted collagenase and hyaluronidase. To evaluate the degradability of these hydrogels, we crosslinked gels modularly using GelNB, GelNB-HPA, PEG4SH, and THA. Prior to enzymatic degradation, we evaluated the stiffness of these gels prior to and after TYR-treatment. As expected, hydrogels crosslinked with GelNB were not sensitive to TYR-triggered stiffening, as demonstrated by their relatively constant moduli (~1 kPa. Fig. 5A). On the other hand, the use of GelNB-HPA rendered the hydrogels sensitive to TYR-triggered on-demand stiffening (Fig. 5A). For example, 1 kU/mL of TYR treatment to gels crosslinked by 0.7 wt% THA led to significant increase of gel moduli from ~1 kPa to 3.5 kPa. Next, soft gels (~1 kPa) or TYR-stiffened gels (~3.5 kPa) were treated with collagenase-1 (40 U/mL, Fig. 5B) or hyaluronidase (300 U/mL, Fig. 5C). In general, stiffened gels degraded slower due to higher crosslinking density contributed by the additional di-HPA linkages [33]. Different from collagenase-mediated degradation where all gels were degraded regardless of stiffness, limited hyaluronidase-mediated degradation was observed (~25% mass loss) in TYR-stiffened gels.

Effect of matrix compositions on PDAC morphological changes

To study the influences of matrix compositions on PDAC cells, we evaluated proliferation and morphology of COLO-357 cells, a PDAC cell line with wild-type *KRAS*, in modularly crosslinked hydrogels, including: (1) GelNB with PEG4SH (Gel/PEG), (2) GelNB with THA (Gel/HA), (3) GelNB-HPA with PEG4SH (Gel_{HPA}/PEG), and (4) GelNB-HPA with THA (Gel_{HPA}/HA). Note that only gels with GelNB-HPA were susceptible to TYR-mediated dynamic stiffening. These gels were formulated such that they had similar initial shear moduli (i.e., 7 wt% GelNB or GelNB-HPA, 1.4 wt% PEG4SH, 0.7 wt% THA. $G' \sim 1$ kPa). Live/dead staining images showed high cell viability after the initial cell encapsulation process and throughout the 14-day *in vitro* culture (Fig. 6A). Cells grew into spheroids or

clusters in all gels but were visibly larger in Gel/PEG hydrogels (i.e., soft and HA-free). Cell proliferation was significantly inhibited (i.e., smaller spheroids) when the hydrogels were soft and contained HA (i.e., Gel/HA) or stiffened but contained no HA (i.e., Gel_{HPA}/PEG). Interestingly, the morphology of the spheroids/clusters in Gel_{HPA}/HA gels became highly irregular (Fig. 6A, right column), an indication of increased cell motility. This could be attributed to higher cell proliferation and/or migration. F-actin staining images also revealed extensive spreading of PDAC cells encapsulated in Gel_{HPA}/HA gels (Fig. 6B).

To quantify changes of spheroid sizes in matrices with different compositions, we analyzed spheroids size from live/dead stained images (Fig. 6C). The average diameter of spheroids was around 20 μm on day 2 in all gels (Fig. S1). Cells encapsulated in soft HA-free matrix (i.e., Gel/PEG) grew into relative large spheroids (~50 μm), whereas the size of cell spheroids in Gel/HA and Gel_{HPA}/PEG gels maintained at around 20–30 μm on day 14 (Fig. S1). As for PDAC cells encapsulated in Gel_{HPA}/HA gels, the spheroids appeared to have similar sizes as the other groups at early days (~20 μm from day 2 to day 7, Fig. 6A). However, due to the highly irregular cell morphology on day 14, we did not analyze cluster sizes in this condition (Fig. 6C).

Analyses of PDAC-related mRNA expression

To gain insight into the influences of microenvironment changes on PDAC cells, we evaluated mRNA expression profiles using TaqMan® Array – Human Pancreatic Adenocarcinoma, which contained pre-deposited primer sets for 92 PDAC-associated and 4 housekeeping genes. Cells were encapsulated in the four groups of hydrogels as described in Fig. 6, following by TYR incubation for 6 hours on day 2 and culturing for additional 12 days (14 days in total). As described before, only gels containing HPA groups would be stiffened. mRNA expression levels were detected using quantitative real time PCR in TaqMan® Array with pre-deposited primers. The expression levels were normalized to GAPDH (housekeeping gene), then to the respective gene in the control group (i.e., Gel/PEG gels). The expression levels of all mRNAs in this group were set as one-fold). mRNA expression levels in the remaining three groups (each with three biological repeats) were ranked from the highest to the lowest fold-changes and then plotted into heat maps (Fig. 7, Table S2, S3). Among the 92 PDAC-related mRNAs, 29, 24, and 48 were up-regulated by more than 2-fold for cells encapsulated in Gel/HA (i.e., soft and with HA), Gel_{HPA}/PEG (i.e., stiffened and HA-free), and Gel_{HPA}/HA (i.e., stiffened and HA-containing) gels, respectively. Furthermore, 52, 48 and 32 mRNAs were down-regulated by more than 2-fold in respective gels. The much higher number of mRNA (i.e., 48) upregulated in the cells encapsulated in Gel_{HPA}/HA gels suggested a potential synergistic effect of HA and a stiffening matrix on PDAC cell progression.

We further examined the expression of genes that were only upregulated in cells encapsulated in stiffened gels (Fig. 8A), in HA-containing gels (Fig. 8B), as well as in stiffened *and* HA-containing gels (Fig. 8C). We found that the expression of MMP2 (encodes matrix metalloproteinase 2), TGF-β3, CCNB1 (encodes Cyclin B1), CCNE2 (encodes Cyclin E2), and E2F3 (encodes E2F transcription factor 3) were significantly upregulated in cells encapsulated in TYR-stiffened gels (Fig. 8A). We also identified

mRNAs that were exclusively upregulated by the presence of HA regardless of matrix stiffness, including FIGF (encodes VEGF-D), ERBB2 (encodes Erb-B2 Receptor Tyrosine Kinase 2), KRAS (encodes K-Ras), SRC (encodes Src), NOTCH1 (encodes Notch-1), BCL2L1 (encodes Bcl-2-Like Protein 1), ELK1 (encodes ETS Transcription Factor), STAT6 (encodes Signal Transducer and Activator of Transcription 6), MAP2K2 (encodes Mitogen-Activated Protein Kinase Kinase 2), and STAT5B (encodes Signal Transducer and Activator of Transcription 5B) (Fig. 8B). Finally, genes that were upregulated only in a stiffened and HA-containing matrix were RAC2 (encodes Small GTP Binding Protein Rac2), TGFβR1 (encodes TGFβ receptor 1), TGF-β2, TP53 (encodes Tumor suppressor P53), NFKB1 (encodes Nuclear Factor $_{K}$B1), AKT1 (encodes serine-threonine protein kinase), RELB (encodes NF-KB Subunit), JAK3 (encodes Janus Kinase 3), CDKN2A (encodes Cyclin Dependent Kinase Inhibitor 2A), EGFR (encodes EGF receptor), RAC1 (encodes Small GTP Binding Protein Rac1), SOS1 (encodes SOS Ras/Rac Guanine Nucleotide Exchange Factor 1), AKT2 (encodes AKT Serine/Threonine Kinase 2), and RHOA (encodes Ras Homolog Family Member A) (Fig. 8C).

Evaluation of relationship between matrices properties and EMT induction

To understand if cell phenotypes observed in Gel_{HPA}/HA gels were a result of matrix-induced EMT (Fig. 6A), we characterized the expression of epithelial and mesenchymal markers (Fig. 9A) using immunostaining and real-time PCR (Fig. 9B). Immunostaining results showed that when the HA-containing hydrogels were dynamically stiffened (i.e., Gel_{HPA}/HA), the expression of epithelial marker E-cadherin (E-cad) decreased drastically (Fig. 9A), whereas the expression of N-cadherin (N-cad, a mesenchymal marker) was visibly noticeable. On the other hand, qPCR results (Fig. 9B) revealed significantly lower level of E-Cad mRNA expression (CDH1, ~0.5-fold), as well as higher expression levels of mesenchymal markers, including N-cad (CDH2, ~2-fold), SNAIL1 (~1.7-fold), vimentin (VIM, ~2.6-fold), and Sonic hedgehog (SHH, ~2.3-fold). Importantly, tyrosinase alone did not cause the observed changes in EMT-related mRNA expressions (Fig. S2). Spreading cell phenotype and upregulation of mesenchymal cell markers in HA-containing/stiffened gels were also obtained using a second PDAC cell line, PANC-1 (Fig. S3). These results demonstrated that EMT was likely the cause of on cell spreading/invasion in the HA-containing gels that had been dynamically stiffened.

Discussion

PDAC microenvironment is a complex network of cells, growth factors, and extracellular matrices whose compositions and properties change significantly as the tumor progresses (Fig. 1). The dynamic changes in the TME pose significant challenges for *in vitro* cancer research and for testing the efficacy of anti-stromal therapeutics. Therefore ideal *in vitro* 3D cell culture platforms for cancer research should have modular and adaptable matrix compositions, as well as dynamically tunable matrix stiffness. Commercial matrices like Matrigel® can provide a convenient 3D culture model but do not have defined compositions and dynamically tunable properties, making it difficult to study the impact of ECM on cancer cell behavior and fate. Alternatively, hydrogels crosslinked by gelatin (Gel) and hyaluronic acid (HA) are increasingly developed as 3D cell culture matrices owing to their

protease degradability and bioactive sequences that are critical in promoting cell proliferation and migration. Besides complex features of ECM composition, accumulating evidence suggest that matrix mechanics is an indispensable parameter regulating cancer cell biology [44-46]. Numerous studies have utilized synthetic hydrogels with tunable stiffness to investigate cancer mechanotransduction. For example, our group has reported Gel/HA hydrogels formed by visible light initiated thiol-norbornene photopolymerization to study the influence of hydrogel crosslinking and compositions on PDAC cell fate [32]. Our earlier efforts have demonstrated that matrix compositions influence the expression of some critical genes related to tumor progression, such as MMP-14, SHH [32], and vascular endothelial growth factors (VEGF) [30]. Moreover, PDAC cells grown in stiffer hydrogels were less susceptible to anti-tumor drugs [10], hence reinforcing the importance of developing an adaptable tumor-mimetic matrix for in vitro cancer research.

The hydrogels developed in the current study integrated modular thiol-norbornene crosslinking (Fig. 1D) [32, 36, 47] with the enzyme-triggered dynamic stiffening strategy (Fig. 1E) that we reported previously [33]. The basic macromer used in this study was gelatin – denatured collagen with enhanced solubility. Native gelatin and modified gelatin macromers are widely used in tissue engineering and regenerative medicine applications owing to its bioactive peptide sequences that permit integrin-binding and protease-triggered degradation [48]. Our lab has also exploited modularly crosslinked gelatin-based hydrogels as 3D cell culture platforms [32, 49-51]. For example, we utilized GelNB as the main functional macromer to construct modular hydrogels for encapsulation and *in vitro* culture of hepatocellular carcinoma (HCC) [49] and PDAC cells [32]. We have also exploited tyrosinase-triggered di-tyrosine crosslinking for dynamically stiffening cell-laden hydrogels and for evaluating its effect on activation of pancreatic stellate cells (PSCs), the major stroma cells in PDAC [33]. Built upon these work, we report here the use of modified gelatin (Fig. 1B, 2), THA (Fig. 1C), and bioinert macromer (e.g., PEG-tetra-thiol, PEG4SH) for constructing gels that were: (1) HA-free and soft (i.e., Gel/PEG gel), (2) HA-free and dynamically stiffened (i.e., Gel_{HPA}/PEG gel), (3) HA-containing and soft (i.e., Gel/HA gel), and (4) HA-containing and dynamically stiffened (i.e., Gel_{HPA}/HA gel). Note that gelatin was used in all gel formulations to provide basic cell adhesion and protease-mediated degradation, whereas only gels composed of GelNB-HPA (i.e., Gel_{HPA}/PEG and Gel_{HPA}/HA) were susceptible to tyrosinase-triggered dynamic stiffening.

We fabricated cell-laden hydrogels with lower thiol-ene ratio but with higher content of GelNB-HPA to obtain gels that were initially soft ($G' < 1$ kPa) but could be stiffened to physiologically-relevant modulus ($G' \sim 3$ kPa. Fig. 3C), akin to what is observed in human PDAC samples and sufficient to induce cell phenotypic and mRNA expression changes [52-55]. As expected, tyrosinase-triggered HPA dimerization increased gel crosslinking and stiffness (Figs. 3C, 3D, 4, Fig. 5A). The degree of gel stiffening was highly tunable owing to the modular crosslinking nature of thiol-norbornene photopolymerization (Fig. 4). While soft hydrogels could be rapidly and completely degraded by collagenase (Fig. 5B) and hyaluronidase (Fig. 5C) within hours, tyrosinase-stiffened hydrogels were less sensitive to these enzymes. When treated with collagenase, degradation followed a surface erosion mechanism regardless of gel stiffness, as indicated by the almost linear mass loss profiles (Fig. 5B). This also applied to hyaluronidase-mediated degradation in soft gels (Fig. 5C).

Exogenously added hyaluronidase, however, did not result in complete degradation of the stiffened gels (only ~ 25% mass loss (Fig. 5C). It was possible that the THA used in this study (from ESI·BIO) had high degree of thiolation, making it difficult for hyaluronidase to cleave HA backbone in a stiffened network. The susceptibility of HA-containing gels to hyaluronidase could be improved by using THA with lower degree of substitution. Nonetheless, all matrices were susceptible to degradation induced by cell-secreted enzymes, a feature critical and necessary in cell-mediated matrix remodeling. It should be noted that these degradation studies were designed to inform the influence of tyrosinase-triggered gel stiffening on subsequent matrix degradation by relevant enzymes (i.e., collagenase and hyaluronidase). The fact that the stiffened gels were susceptible to exogenously added enzymes (especially collagenase) suggests that the encapsulated PDAC cells would still be able to degrade stiffened matrix locally, hence facilitating their proliferation, invasion, and migration.

The changes in cell morphology among different gel formulations and stiffening conditions indicated that 3D matrix composition exerts a profound impact on PDAC cell fate. Through modular control of gel compositions and dynamic stiffening, we show that the presence of HA in a soft gel (i.e., Gel/HA) *or* an HA-free but stiffened gel (i.e., Gel_{HPA}/PEG) hindered the growth of PDAC cells in 3D (Fig. 6), underscoring the complex relationship between cell proliferation, HA levels, and TME stiffness. On the other hand, smaller spheroids observed in the stiffened and HA-free gel could be a result of stress-induced signaling and physical restriction imposed by tighter network crosslinking after stiffening. We have observed a similar phenomenon in PDAC cells using hydrogels with higher but static stiffness [32]. However, the negative impact of network-immobilized HA on spheroid sizes was surprising since HA has been shown to induce PDAC cell proliferation in 2D culture [56]. The suppression of spheroid growth compared with that in soft and HA-free gel (i.e., Gel/PEG) could be due to the dependence of HA-mediated mitogenic signaling on matrix stiffness. Interestingly, when cells were grown in HA-containing *and* stiffened gels (i.e., Gel_{HPA}/HA), significant cell spreading was observed (Fig. 6A, 6B). This could be attributed to the upregulation of mRNAs implicated in the Ras/MAPK pathway, including RAC1, RAC2, RHOA, and RAF1 (Fig. 7B), and EMT-induced alterations. The upregulation of these mRNAs could lead to enhanced proliferation and to increased cell migration/invasion as observed in the stiffened and HA-containing hydrogel.

We also identified mRNAs that were upregulated only when the cells were encapsulated in stiffened gels (Fig. 8A), in HA-containing gels (Fig. 8B), or in HA-containing *and* stiffened gel (Fig. 8C). We found that FIGF, ELK1, KRAS, SRC, and NOTCH1 were upregulated in cells grown in HA-containing gels, and that their expression was further upregulated when combined with gel stiffening. These findings are of crucial importance for several reasons. First, increased expression of KRAS and SRC is known to enhance tumorigenesis and metastasis [52, 57], and here we show for the first time that their expression is upregulated by key features found in the PDAC TME. Second, the upregulation of FIGF likely leads to increased levels of VEGF-D, which is known to promote lymph node metastasis in PDAC [58, 59]. Third, NOTCH1 encodes Notch 1, whose activation correlates with increased drug resistance in PDAC [60-62].

Another interesting phenomenon is the elevated expression of MMPs, which are involved in ECM degradation and cancer cell invasion [63, 64]. We noted high levels of MMP7, the smallest member of the MMP family yet endowed with high proteolytic activity [65], in all experimental groups (compared to that in Gel/PEG hydrogel). On the other hand, MMP2 was only highly expressed in gels that were stiffened dynamically regardless of HA presence (Fig. 8A). These findings suggest that our modular and dynamic hydrogels are ideal for future studies regarding the influence of matrix components on the expression and activity of MMPs or as an adaptable platform to test the efficacy of anti-MMP therapeutics. Furthermore, in a stiffened tumor-mimetic hydrogel, HA was found to upregulate mRNAs responsible for enhancing cancer cell survival and drug resistance (i.e., AKT1, AKT2, PIK2R1, PIK3R2, NFKNB1, and RELB. Fig. 7, 8C).

Additional genes in the EGF and TGF-β pathways were significantly upregulated only in the setting of a stiffened and HA-containing microenvironment. These genes included TGFβR1, TGF-β2, and EGFR (Fig. 8C). Moreover, TGF-β3 was upregulated in the setting of a stiffened gel and further upregulated when combined with HA (Fig. 8A). These signaling events may collaboratively lead to enhanced EMT in PDAC cells (Fig. 9). In addition, these observations underscore the fact that EGFR and TGF-β pathways are known to cross-talk in the context of upregulated Kras activity, thereby lead to autocrine dysregulation that promotes invasion and metastasis, as well as to aberrant paracrine actions that contribute to the desmosplasia in the TME and that impair cancer-directed immune mechanisms [66, 67]. While previous efforts have led to current understanding of soluble factors (e.g., growth factors, cytokines, soluble HA) on PDAC cell growth and EMT, the influence of 3D matrix compositions and time-dependent mechanics on PDAC cell fate remains elusive owing to the lack of a modular and adaptable biomimetic culture platform.

Although the Gel_{HPA}/HA gel system developed here only recapitulate certain aspects of the complex PDAC stroma, it nonetheless provides a highly relevant dynamic biomaterial platform for studying tumor cell-materials interactions in a reductionistic manner. Pancreatic cancer desmosplasia is undoubtedly highly complex. Precisely because of this complexity, it is important to establish model systems that allow for the reductionist dissection of specific components within the desmosplasia to understand how they contribute to pancreatic cancer pathobiology. In this contribution, we report the unique synergistic roles of HA and a stiffening matrix on PDAC cell behaviors, which has not been reported before. Accordingly, we document that HA and a stiffening matrix can lead to enhanced expression of KRAS and SRC, both of which are crucial contributors to pancreatic cancer aggressiveness, as well as increased VEGF-D and Notch 1 expression which promote lymph node metastasis and chemoresistance, respectively. Collectively, these changes can lead to enhanced EMT in pancreatic cancer. The results presented here provide insight that could lead to novel therapeutic approaches based on targeting HA in combination of components of the above pathways. Built upon the current system, other stroma-relevant components (e.g., fibronectin, laminin) may be added in future studies to understand the crosstalk between these stroma components and matrix mechanics on PDAC cell fate processes. Finally, the enzyme-responsive matrix stiffening approach is highly cytocompatible, controllable, and adaptable for creating cell-laden gels with spatial-temporally regulated stiffness. Our on-

going work is focused on generating biomimetic gels with stiffness gradient to evaluate durotatic cell migration and invasion in 3D.

Conclusion

In conclusion, we have designed a biomimetic hydrogel capable of mimicking the diverse biochemical compositions and dynamic biophysical environment of pancreatic desmoplasia. The modular thiol-norbornene crosslinking of gelatin, HA, and PEG-based macromers decoupled the influence of HA and matrix stiffness on PDAC cell fate. Furthermore, the inclusion of HPA motif rendered the gels responsive to tyrosinase-triggered HPA dimerization and additional gel crosslinking. Through modular design, the hydrogels could be stiffened with high controllability. PDAC cells responded to the stiffening or HA-containing gel with limited cell proliferation. On the other hand, we confirmed that HA and matrix stiffening synergistically promoted invasive and matrix-induced EMT phenotype in PDAC cells. The desmoplasia-mimetic hydrogel developed here provides a diverse material platform for studying PDAC cell fate. Future work will focus on utilizing this versatile system for investigating cellular response to therapeutics under various matrix composition and mechanical properties.

Supplementary Material

Refer to Web version on PubMed Central for supplementary material.

Acknowledgments

This work was supported in part by the National Cancer Institute (NCI) of the National Institutes of Health (R21CA188911 to C.C. Lin, R01CA075059 to M. Korc) and National Science Foundation (CAREER Award, DMR #1452390 to C.C. Lin).

References

1. Siegel RL, Miller KD, Jemal A. Cancer Statistics, 2017. CA Cancer J Clin. 2017; 67(1):7–30. [PubMed: 28055103]
2. Kleeff J, Korc M, Apte M, La Vecchia C, Johnson CD, Biankin AV, Neale RE, Tempero M, Tuveson DA, Hruban RH, Neoptolemos JP. Pancreatic cancer. Nature reviews Disease primers. 2016; 2:16022.
3. Chanmee T, Ontong P, Itano N. Hyaluronan: A modulator of the tumor microenvironment. Cancer Lett. 2016; 375(1):20–30. [PubMed: 26921785]
4. Kota J, Hancock J, Kwon J, Korc M. Pancreatic cancer: Stroma and its current and emerging targeted therapies. Cancer Lett. 2017; 391:38–49. [PubMed: 28093284]
5. Haqq J, Howells LM, Garcea G, Metcalfe MS, Steward WP, Dennison AR. Pancreatic stellate cells and pancreas cancer: current perspectives and future strategies. Eur J Cancer. 2014; 50(15):2570–2582. [PubMed: 25091797]
6. Korc M. Pancreatic cancer-associated stroma production. Am J Surg. 2007; 194(4 Suppl):S84–86. [PubMed: 17903452]
7. Zheng X, Carstens JL, Kim J, Scheible M, Kaye J, Sugimoto H, Wu CC, LeBleu VS, Kalluri R. Epithelial-to-mesenchymal transition is dispensable for metastasis but induces chemoresistance in pancreatic cancer. Nature. 2015; 527(7579):525–530. [PubMed: 26560028]
8. Polireddy K, Chen Q. Cancer of the Pancreas: Molecular Pathways and Current Advancement in Treatment. J Cancer. 2016; 7(11):1497–1514. [PubMed: 27471566]

9. Jung HY, Fattet L, Yang J. Molecular pathways: linking tumor microenvironment to epithelial-mesenchymal transition in metastasis. Clin Cancer Res. 2015; 21(5):962–968. [PubMed: 25107915]
10. Ki CS, Shih H, Lin CC. Effect of 3D matrix compositions on the efficacy of EGFR inhibition in pancreatic ductal adenocarcinoma cells. Biomacromolecules. 2013; 14(9):3017–3026. [PubMed: 23889305]
11. Sempere LF, Gunn JR, Korc M. A novel 3-dimensional culture system uncovers growth stimulatory actions by TGFbeta in pancreatic cancer cells. Cancer biology & therapy. 2011; 12(3): 198–207. [PubMed: 21613822]
12. Gore J, Korc M. Pancreatic cancer stroma: Friend or foe? Cancer Cell. 2014; 25(6):711–712. [PubMed: 24937454]
13. Lamouille S, Xu J, Derynck R. Molecular mechanisms of epithelial-mesenchymal transition. Nat Rev Mol Cell Biol. 2014; 15(3):178–196. [PubMed: 24556840]
14. Zeisberg M, Neilson EG. Biomarkers for epithelial-mesenchymal transitions. J Clin Invest. 2009; 119(6):1429–1437. [PubMed: 19487819]
15. Castellanos JA, Merchant NB, Nagathihalli NS. Emerging targets in pancreatic cancer: epithelial-mesenchymal transition and cancer stem cells. Onco Targets Ther. 2013; 6:1261–1267. [PubMed: 24049451]
16. Wang Z, Li Y, Ahmad A, Banerjee S, Azmi AS, Kong D, Sarkar FH. Pancreatic cancer: understanding and overcoming chemoresistance. Nat Rev Gastroenterol Hepatol. 2011; 8(1):27–33. [PubMed: 21102532]
17. Egeblad M, Rasch MG, Weaver VM. Dynamic interplay between the collagen scaffold and tumor evolution. Curr Opin Cell Biol. 2010; 22(5):697–706. [PubMed: 20822891]
18. Wei SC, Fattet L, Tsai JH, Guo Y, Pai VH, Majeski HE, Chen AC, Sah RL, Taylor SS, Engler AJ, Yang J. Matrix stiffness drives epithelial-mesenchymal transition and tumour metastasis through a TWIST1-G3BP2 mechanotransduction pathway. Nat Cell Biol. 2015; 17(5):678–688. [PubMed: 25893917]
19. Gurski LA, Xu X, Labrada LN, Nguyen NT, Xiao L, van Golen KL, Jia X, Farach-Carson MC. Hyaluronan (HA) interacting proteins RHAMM and hyaluronidase impact prostate cancer cell behavior and invadopodia formation in 3D HA-based hydrogels. PLoS One. 2012; 7(11):e50075. [PubMed: 23166824]
20. Toole BP. Hyaluronan: from extracellular glue to pericellular cue. Nat Rev Cancer. 2004; 4(7):528–539. [PubMed: 15229478]
21. Borowsky ML, Hynes RO. Layilin, A Novel Talin-binding Transmembrane Protein Homologous with C-type Lectins, is Localized in Membrane Ruffles. 1998
22. Gotte M, Yip GW. Heparanase, hyaluronan, and CD44 in cancers: a breast carcinoma perspective. Cancer Res. 2006; 66(21):10233–10237. [PubMed: 17079438]
23. Javle M, Golan T, Maitra A. Changing the course of pancreatic cancer–Focus on recent translational advances. Cancer Treat Rev. 2016; 44:17–25. [PubMed: 26924195]
24. Sironen RK, Tammi M, Tammi R, Auvinen PK, Anttila M, Kosma VM. Hyaluronan in human malignancies. Exp Cell Res. 2011; 317(4):383–391. [PubMed: 21134368]
25. Kirschner CM, Anseth KS. Hydrogels in Healthcare: From Static to Dynamic Material Microenvironments. Acta Mater. 2013; 61(3):931–944. [PubMed: 23929381]
26. Stowers RS, Allen SC, Suggs LJ. Dynamic phototuning of 3D hydrogel stiffness. Proc Natl Acad Sci U S A. 2015; 112(7):1953–1958. [PubMed: 25646417]
27. Paszek MJ, Zahir N, Johnson KR, Lakins JN, Rozenberg GI, Gefen A, Reinhart-King CA, Margulies SS, Dembo M, Boettiger D, Hammer DA, Weaver VM. Tensional homeostasis and the malignant phenotype. Cancer Cell. 2005; 8(3):241–254. [PubMed: 16169468]
28. Chaudhuri O, Koshy ST, Branco da Cunha C, Shin JW, Verbeke CS, Allison KH, Mooney DJ. Extracellular matrix stiffness and composition jointly regulate the induction of malignant phenotypes in mammary epithelium. Nat Mater. 2014; 13(10):970–978. [PubMed: 24930031]
29. Xu W, Qian J, Zhang Y, Suo A, Cui N, Wang J, Yao Y, Wang H. A double-network poly(Nvarepsilon-acryloyl L-lysine)/hyaluronic acid hydrogel as a mimic of the breast tumor microenvironment. Acta Biomater. 2016; 33:131–141. [PubMed: 26805429]

30. Ki CS, Lin TY, Korc M, Lin CC. Thiol-ene hydrogels as desmoplasia-mimetic matrices for modeling pancreatic cancer cell growth, invasion, and drug resistance. Biomaterials. 2014; 35(36): 9668–9677. [PubMed: 25176061]
31. Raza A, Ki CS, Lin CC. The influence of matrix properties on growth and morphogenesis of human pancreatic ductal epithelial cells in 3D. Biomaterials. 2013; 34(21):5117–5127. [PubMed: 23602364]
32. Shih H, Greene T, Korc M, Lin CC. Modular and Adaptable Tumor Niche Prepared from Visible Light Initiated Thiol-Norbornene Photopolymerization. Biomacromolecules. 2016; 17(12):3872–3882. [PubMed: 27936722]
33. Liu HY, Greene T, Lin TY, Dawes CS, Korc M, Lin CC. Enzyme-mediated stiffening hydrogels for probing activation of pancreatic stellate cells. Acta Biomater. 2017; 48:258–269. [PubMed: 27769941]
34. Mũnoz Z, Shih H, Lin CC. Gelatin hydrogels formed by orthogonal thiol–norbornene photochemistry for cell encapsulation. Biomater Sci. 2014; 2(8):1063–1072.
35. Wang Y, Wang J. Mixed hydrogel bead-based tumor spheroid formation and anticancer drug testing. Analyst. 2014; 139(10):2449–2458. [PubMed: 24699505]
36. Lin CC, Ki CS, Shih H. Thiol-norbornene photoclick hydrogels for tissue engineering applications. Journal of Applied Polymer Science. 2015; 132(8):41563. [PubMed: 25558088]
37. Lin CC, Raza A, Shih H. PEG hydrogels formed by thiol-ene photo-click chemistry and their effect on the formation and recovery of insulin-secreting cell spheroids. Biomaterials. 2011; 32(36): 9685–9695. [PubMed: 21924490]
38. Lin TY, Bragg JC, Lin CC. Designing Visible Light-Cured Thiol-Acrylate Hydrogels for Studying the HIPPO Pathway Activation in Hepatocellular Carcinoma Cells. Macromol Biosci. 2016; 16(4): 496–507. [PubMed: 26709469]
39. Wang LS, Chung JE, Chan PP, Kurisawa M. Injectable biodegradable hydrogels with tunable mechanical properties for the stimulation of neurogenesic differentiation of human mesenchymal stem cells in 3D culture. Biomaterials. 2010; 31(6):1148–1157. [PubMed: 19892395]
40. Hu M, Kurisawa M, Deng R, Teo CM, Schumacher A, Thong YX, Wang L, Schumacher KM, Ying JY. Cell immobilization in gelatin-hydroxyphenylpropionic acid hydrogel fibers. Biomaterials. 2009; 30(21):3523–3531. [PubMed: 19328545]
41. Eastoe JE. The amino acid composition of mammalian collagen and gelatin. Biochem J. 1955; 61(4):589–600. [PubMed: 13276342]
42. Fenoll LG, Rodriguez-Lopez JN, Garcia-Sevilla F, Garcia-Ruiz PA, Varon R, Garcia-Canovas F, Tudela J. Analysis and interpretation of the action mechanism of mushroom tyrosinase on monophenols and diphenols generating highly unstable o-quinones. Biochim Biophys Acta. 2001; 1548(1):1–22. [PubMed: 11451433]
43. Nguyen AV, Nyberg KD, Scott MB, Welsh AM, Nguyen AH, Wu N, Hohlbauch SV, Geisse NA, Gibb EA, Robertson AG, Donahue TR, Rowat AC. Stiffness of pancreatic cancer cells is associated with increased invasive potential. Integr Biol (Camb). 2016; 8(12):1232–1245. [PubMed: 27761545]
44. Rath N, Olson MF. Regulation of pancreatic cancer aggressiveness by stromal stiffening. Nat Med. 2016; 22(5):462–463. [PubMed: 27149218]
45. Brancato V, Comunanza V, Imparato G, Cora D, Urciuolo F, Noghero A, Bussolino F, Netti PA. Bioengineered tumoral microtissues recapitulate desmoplastic reaction of pancreatic cancer. Acta Biomater. 2017; 49:152–166. [PubMed: 27916739]
46. Laklai H, Miroshnikova YA, Pickup MW, Collisson EA, Kim GE, Barrett AS, Hill RC, Lakins JN, Schlaepfer DD, Mouw JK, LeBleu VS, Roy N, Novitskiy SV, Johansen JS, Poli V, Kalluri R, Iacobuzio-Donahue CA, Wood LD, Hebrok M, Hansen K, Moses HL, Weaver VM. Genotype tunes pancreatic ductal adenocarcinoma tissue tension to induce matricellular fibrosis and tumor progression. Nat Med. 2016; 22(5):497–505. [PubMed: 27089513]
47. Lin CC. Recent advances in crosslinking chemistry of biomimetic poly(ethylene glycol) hydrogels. RSC Adv. 2015; 5(50):39844–398583. [PubMed: 26029357]

48. Yue K, Trujillo-de Santiago G, Alvarez MM, Tamayol A, Annabi N, Khademhosseini A. Synthesis, properties, and biomedical applications of gelatin methacryloyl (GelMA) hydrogels. Biomaterials. 2015; 73:254–271. [PubMed: 26414409]
49. Greene T, Lin CC. Modular cross-linking of gelatin-based thiol-norbornene hydrogels for in vitro 3D culture of hepatocellular carcinoma cells. ACS Biomaterials Science & Engineering. 2015; 1(12):1314–1323.
50. Munoz Z, Shih H, Lin CC. Gelatin hydrogels formed by orthogonal thiol-norbornene photochemistry for cell encapsulation. Biomaterials Science. 2014; 2(8):1063–1072.
51. Greene T, Lin TY, Andrisani OM, Lin CC. Comparative study of visible light polymerized gelatin hydrogels for 3D culture of hepatic progenitor cells. Journal of Applied Polymer Science. 2017; 134(11)
52. Rubiano A, Delitto D, Han S, Gerber M, Galitz C, Trevino J, Thomas RM, Hughes SJ, Simmons CS. Viscoelastic properties of human pancreatic tumors and in vitro constructs to mimic mechanical properties. Acta Biomater. 2017
53. Arda K, Ciledag N, Aktas E, Aribas BK, Kose K. Quantitative assessment of normal soft-tissue elasticity using shear-wave ultrasound elastography. AJR Am J Roentgenol. 2011; 197(3):532–536. [PubMed: 21862792]
54. Rice AJ, Cortes E, Lachowski D, Cheung BCH, Karim SA, Morton JP, Del Rio Hernandez A. Matrix stiffness induces epithelial-mesenchymal transition and promotes chemoresistance in pancreatic cancer cells. Oncogenesis. 2017; 6(7):e352. [PubMed: 28671675]
55. Lachowski D, Cortes E, Pink D, Chronopoulos A, Karim SA, J PM, Del Rio Hernandez AE. Substrate Rigidity Controls Activation and Durotaxis in Pancreatic Stellate Cells. Sci Rep. 2017; 7(1):2506. [PubMed: 28566691]
56. Sato N, Kohi S, Hirata K, Goggins M. Role of hyaluronan in pancreatic cancer biology and therapy: Once again in the spotlight. Cancer Sci. 2016; 107(5):569–575. [PubMed: 26918382]
57. di Magliano MP, Logsdon CD. Roles for KRAS in pancreatic tumor development and progression. Gastroenterology. 2013; 144(6):1220–1229. [PubMed: 23622131]
58. Kurahara H, Takao S, Maemura K, Shinchi H, Natsugoe S, Aikou T. Impact of vascular endothelial growth factor-C and -D expression in human pancreatic cancer: its relationship to lymph node metastasis. Clin Cancer Res. 2004; 10(24):8413–8420. [PubMed: 15623620]
59. Gore J, Imasuen-Williams IE, Conteh AM, Craven KE, Cheng M, Korc M. Combined targeting of TGF-beta, EGFR and HER2 suppresses lymphangiogenesis and metastasis in a pancreatic cancer model. Cancer Lett. 2016; 379(1):143–153. [PubMed: 27267807]
60. Wang Z, Li Y, Kong D, Banerjee S, Ahmad A, Azmi AS, Ali S, Abbruzzese JL, Gallick GE, Sarkar FH. Acquisition of epithelial-mesenchymal transition phenotype of gemcitabine-resistant pancreatic cancer cells is linked with activation of the notch signaling pathway. Cancer Res. 2009; 69(6):2400–2407. [PubMed: 19276344]
61. Ristorcelli E, Lombardo D. Targeting Notch signaling in pancreatic cancer. Expert Opin Ther Targets. 2010; 14(5):541–552. [PubMed: 20392166]
62. Gungor C, Zander H, Effenberger KE, Vashist YK, Kalinina T, Izbicki JR, Yekebas E, Bockhorn M. Notch signaling activated by replication stress-induced expression of midkine drives epithelial-mesenchymal transition and chemoresistance in pancreatic cancer. Cancer Res. 2011; 71(14): 5009–5019. [PubMed: 21632553]
63. Shields MA, Dangi-Garimella S, Redig AJ, Munshi HG. Biochemical role of the collagen-rich tumour microenvironment in pancreatic cancer progression. Biochem J. 2012; 441(2):541–552. [PubMed: 22187935]
64. Lunardi S, Muschel RJ, Brunner TB. The stromal compartments in pancreatic cancer: are there any therapeutic targets? Cancer Lett. 2014; 343(2):147–155. [PubMed: 24141189]
65. Jakubowska K, Pryczynicz A, Januszewska J, Sidorkiewicz I, Kemona A, Niewinski A, Lewczuk L, Kedra B, Guzinska-Ustymowicz K. Expressions of Matrix Metalloproteinases 2, 7, and 9 in Carcinogenesis of Pancreatic Ductal Adenocarcinoma. Disease Markers. 2016; 2016:9895721. [PubMed: 27429508]

66. Grusch M, Petz M, Metzner T, Ozturk D, Schneller D, Mikulits W. The crosstalk of RAS with the TGF-beta family during carcinoma progression and its implications for targeted cancer therapy. Curr Cancer Drug Targets. 2010; 10(8):849–857. [PubMed: 20718708]

67. Kang M, Choi S, Jeong SJ, Lee SA, Kwak TK, Kim H, Jung O, Lee MS, Ko Y, Ryu J, Choi YJ, Jeong D, Lee HJ, Ye SK, Kim SH, Lee JW. Cross-talk between TGFbeta1 and EGFR signalling pathways induces TM4SF5 expression and epithelial-mesenchymal transition. Biochem J. 2012; 443(3):691–700. [PubMed: 22292774]

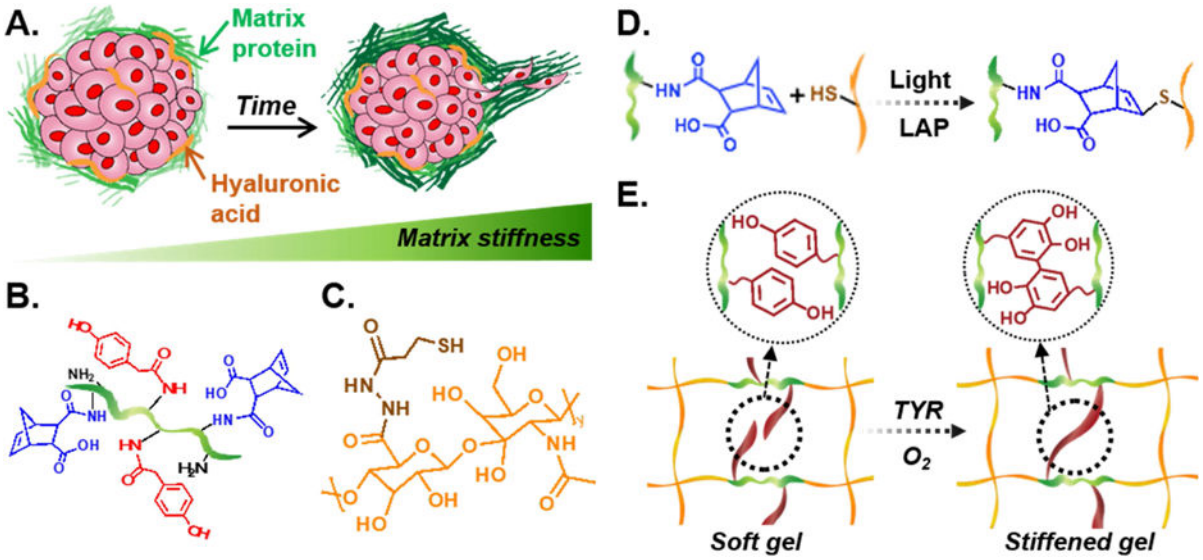

Figure 1. Enzyme-triggered on-demand stiffening of biomimetic hydrogels for *in vitro* cancer cell research

(A) Schematic of a tumor microenvironment with various matrix proteins and glycosaminoglycans (e.g., HA). Accumulation of these ECM leads to matrix stiffening and tumor progression. (B) Chemical structure of GelNB-HPA, (C) Chemical structure of THA. (D) Schematic of light and photoinitiator (LAP) induced thiol-norbornene crosslinking. (E) Schematic of tyrosinase-triggered di-HPA crosslinking and on-demand hydrogel stiffening.

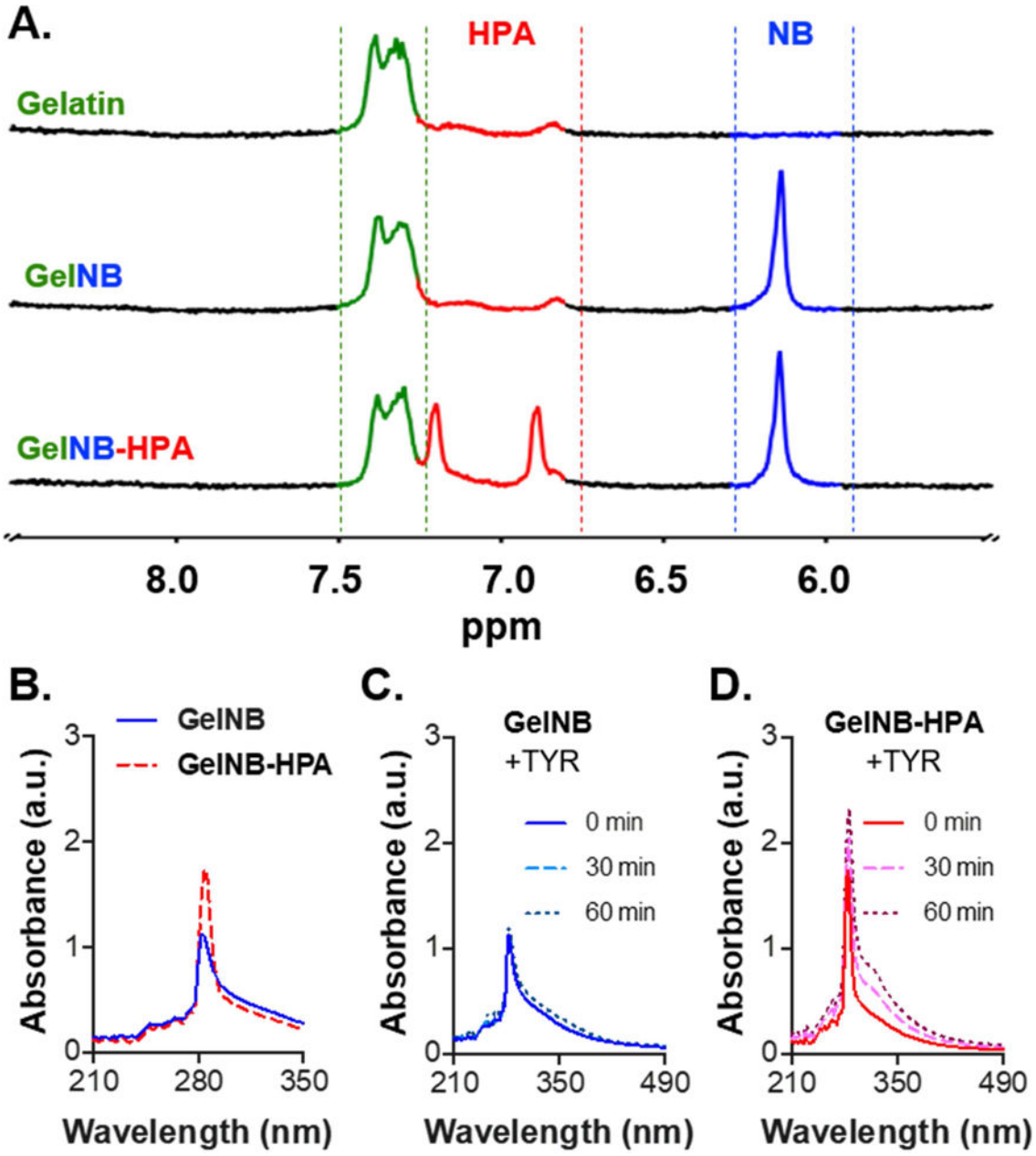

Figure 2. Characterizaiton of functionalized gelatin macromers

(A) ^{1}NMR spectra of Gelatin, GelNB, and GelNB-HPA. (B-D) UV/Vis absorbance spectra of soluble GelNB and GelNB-HPA (A), soluble GelNB treated with tyrosinase (TYR, 1 kU/mL) (C), and soluble GelNB-HPA treated with TYR (D).

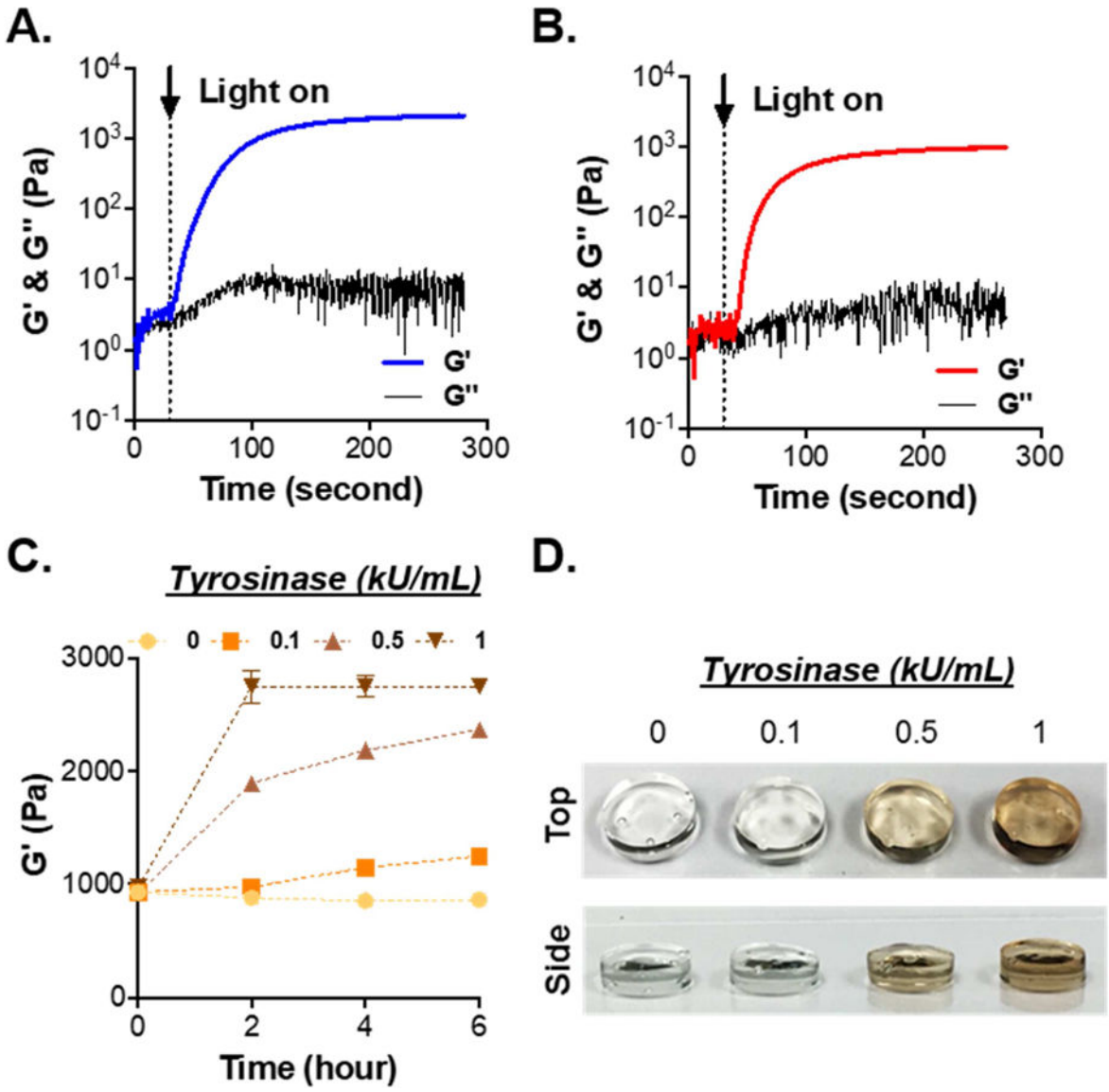

Figure 3. Characterization of thiol-norbornene gelation using functionalized gelation macromers

(A, B) Evolution of storage (G′) and loss (G″) moduli of thiol-norbornene gelation using Gel/PEG (A) and Gel_{HPA}/PEG (B). GelNB or GelNB-HPA was added at 7 wt%, whereas PEG4SH was added at 1.4 wt% (R=0.5). (C) On-demand stiffening of Gel/PEG hydrogels via adding TYR at different concentrations (N=3, Mean ± SEM). (D) Photograph of tyrosinase-stiffened hydrogels.

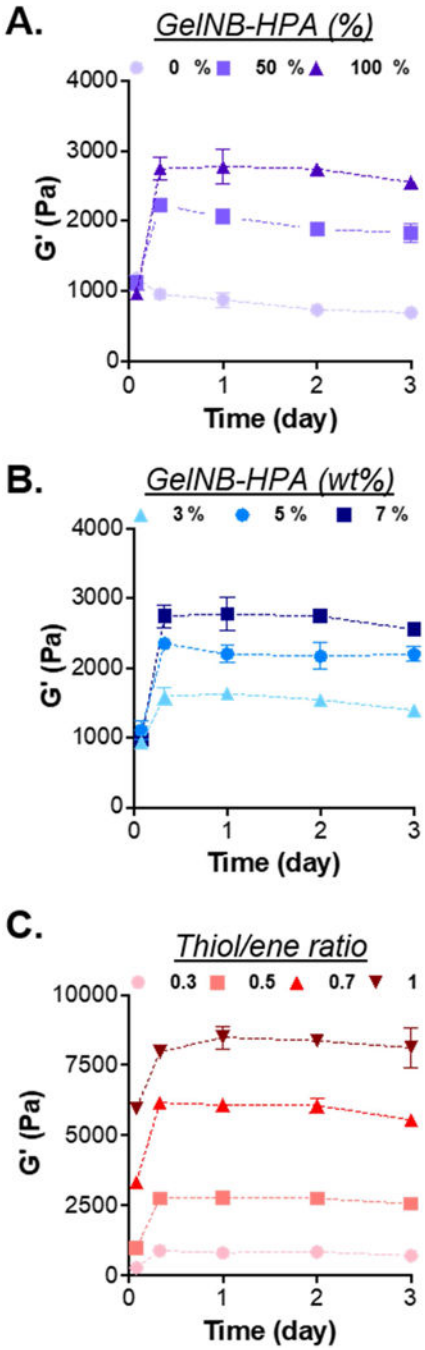

Figure 4. Effect of macromer compositions on TYR-triggered on-demand gel stiffening

(A) Shear moduli of hydrogels formed by 7 wt% of gelatin macromer (GelNB and/or GelNB-HPA) and 1.4 wt% PEG4SH. Gels were formed with different fractions of GelNB-HPA and GelNB. (B) Shear moduli of hydrogels formed by 3, 5, or 7 wt% of GelNB-HPA and with 0.7 wt% of PEG4SH, yielding gels with varied HPA contents but with similar initial modulus. (C) Shear moduli of hydrogels formed by 7 wt% of GelNB-HPA but with varied PEG4SH content to yield thiol/ene ratio of 0.3, 0.5, 0.7, 1. These gels contained the

same HPA content but different initial modulus. All hydrogels were treated with 1 kU/mL TYR from 0 – 6 hours (N=3, Mean ± SEM).

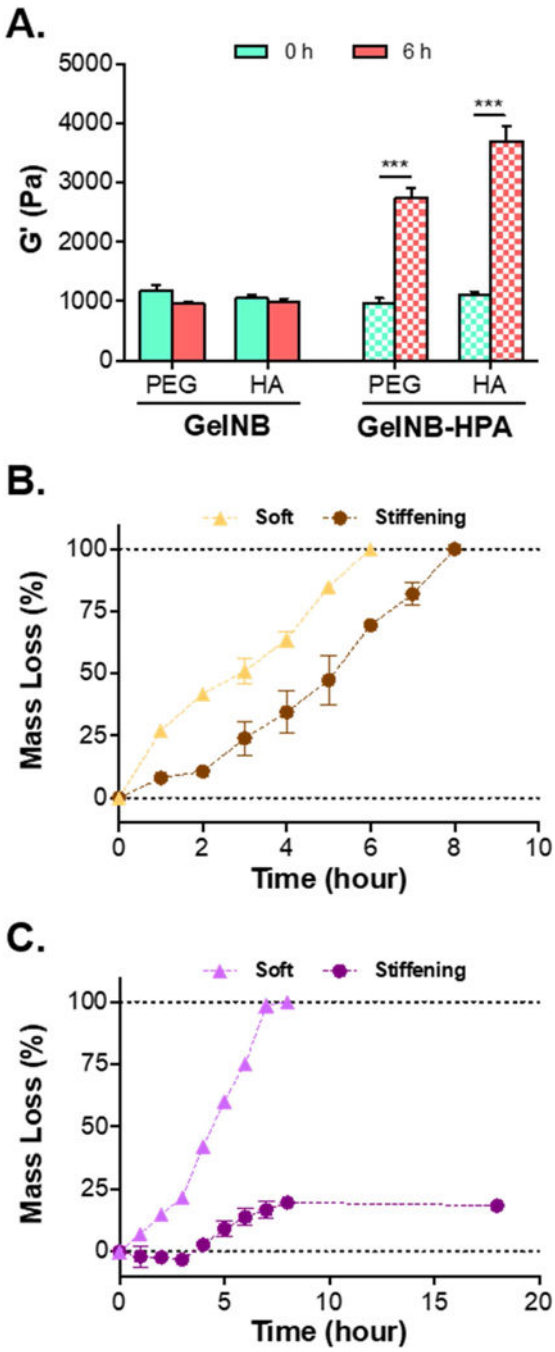

Figure 5. Effect of tyrosinase-mediated gel stiffening on enzyme-mediated degradation

(A) Comparison of modulus changes in hydrogels modularly crosslinked by GelNB or GelNB-HPA with PEG4SH or THA. Gel moduli were characterized prior to and after treating with 1 kU/mL TYR for 6 hours (***$p < 0.001$). (B) Mass loss profiles of Gel/HA (soft) or Gel_{HPA}/HA (TYR-stiffened) hydrogels treated with collagenase (40 U/mL). (C) Mass loss profiles of Gel/HA (soft) or Gel_{HPA}/HA (TYR-stiffened) hydrogels treated with hyaluronidase (300 U/mL). Hydrogels in (B) and (C) were formed by 7% GelNB or GelNB-HPA with 0.7% THA (N=3, Mean ± SEM).

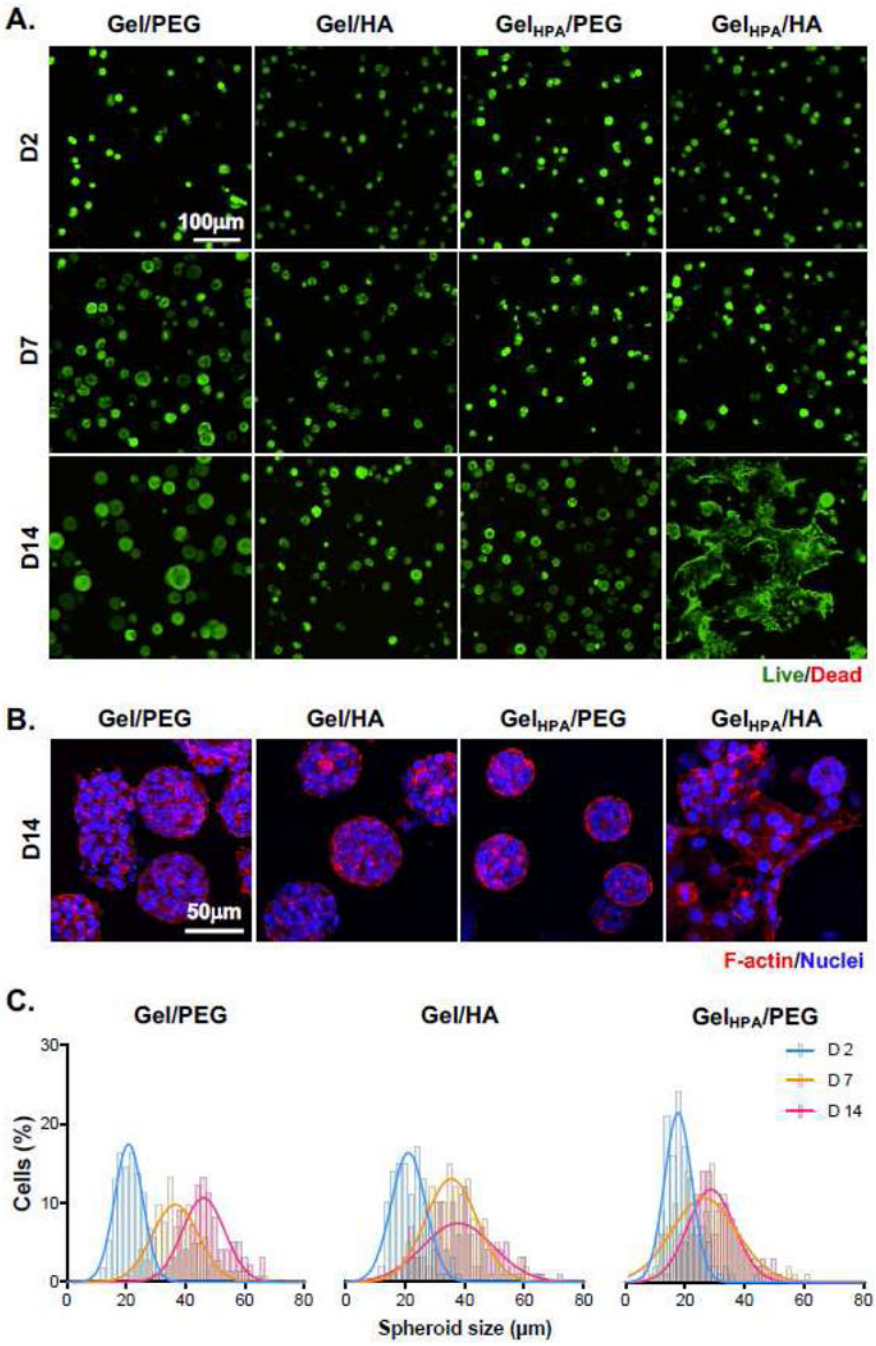

Figure 6. Effect of matrix compositions on morphological changes of COLO-357 cells

(A) Representative confocal z-stack live/dead stained images of cells in Gel/PEG, Gel/HA, Gel$_{HPA}$/PEG, and Gel$_{HPA}$/HA gels. Gels were incubated with tyrosinase for 6 hours at day 2 and transferred to fresh media. (B) Confocal z-stack images of F-actin staining of encapsulated cells on day 14 post-encapsulation. Cell nuclei were counter-stained with DAPI. (C) Cell spheroid diameters as a function of time and hydrogel formulations. Histograms were fitted with Gaussian distribution.

Figure 7. Effect of matrix compositions on PDAC-related gene expression in COLO-357 cells

Heat maps of Taqman® array analyses of gene expression in cells encapsulated in Gel/PEG (control group, data not shown in the figure as expression levels of all genes were set as one-fold), Gel/HA, Gel$_{HPA}$/PEG, and Gel$_{HPA}$/HA hydrogels. Gene expression levels (plotted in Log$_2$ scale) were normalized to GAPDH within each group, then normalized to respective gene in Gel/PEG hydrogels. Each of the four gel formulations contained three biological replicates. Warm (red) colors showed high expression, whereas cold (blue) colors showed low expression.

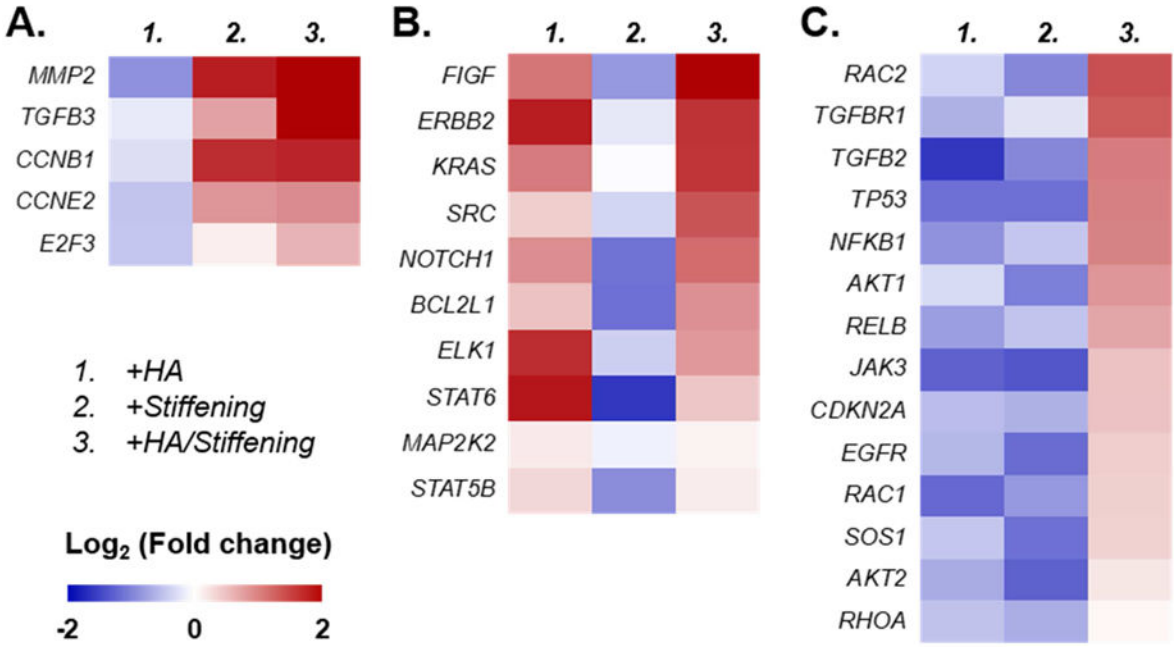

Figure 8. Identification of genes that were upregulated in COLO-357 cells encapsulated in specific gel formulations

(A) Stiffening gel regardless of HA presence, (B) HA-containing gel regardless of gel stiffening, and (C) HA-containing and stiffened gel. Gene expression levels (plotted in Log_2 scale) were normalized to GAPDH within each group, then normalized to respective gene in Gel/PEG hydrogels. Each of the four gel formulations contained three biological replicates. Warm (red) colors showed high expression, whereas cold (blue) colors showed low expression.

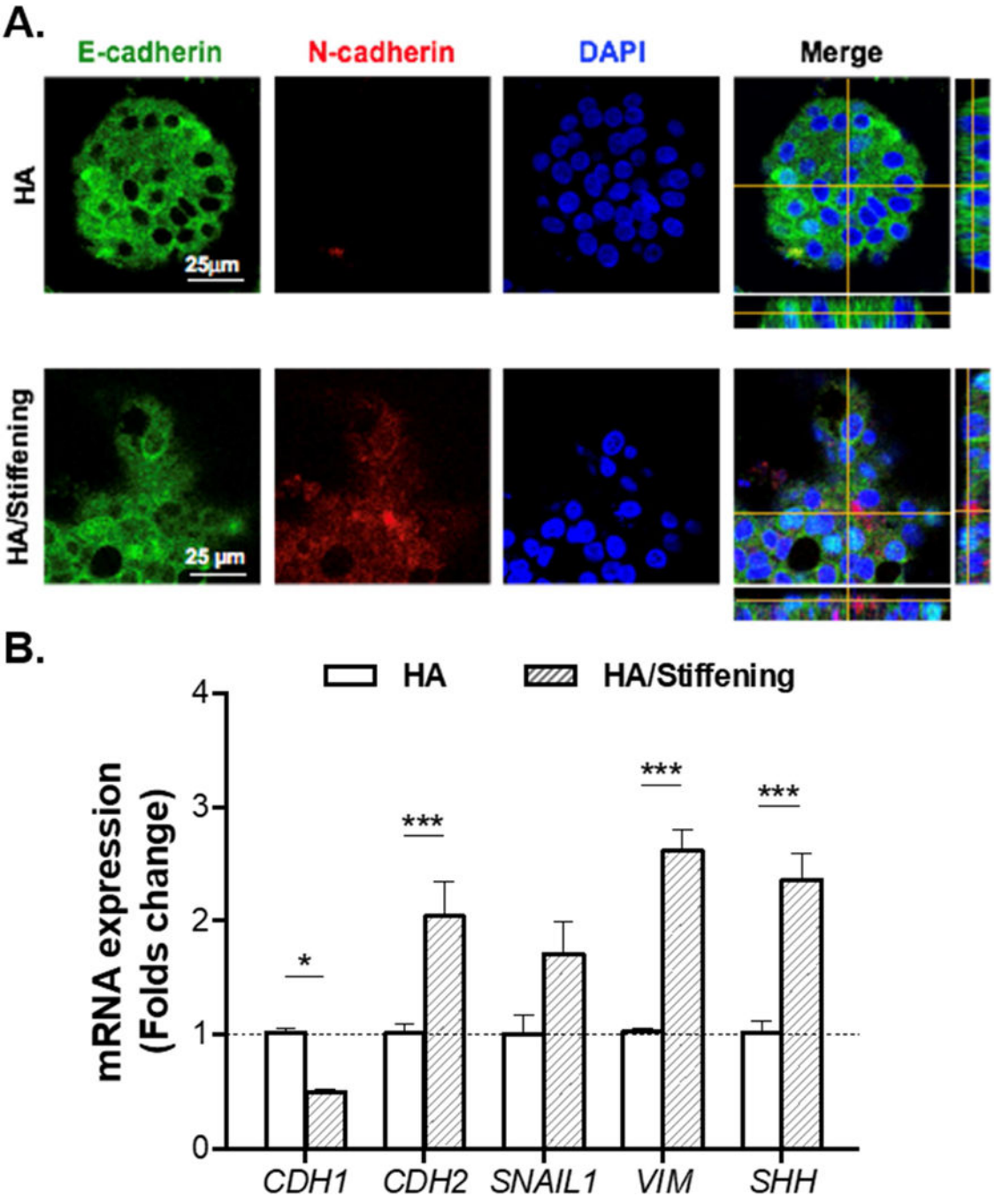

Figure 9. Evaluation of selected epithelial and mesenchymal markers in COLO-357 cells grown in HA-containing and soft (i.e., Gel/HA) or in HA-containing and TYR-stiffened gels (i.e., Gel_{HPA}/HA)

(A) Immunofluorescence staining of E-cadherin and N-cadherin. Cells were counterstained with DAPI. (B) mRNA expression levels of CDH1 (E-cadherin), CDH2 (N-cadherin), SNAIL1, VIM (vimentin), and SHH (sonic hedgehog). All assays were conducted with samples collected at day 14. (Housekeeping gene: GAPDH. N=3, Mean ± SEM. *p<0.05, ***p<0.001).